



Remarkable positive effect of Cd(OH)₂ on CdS semiconductor for visible-light photocatalytic H₂ production

Qin Li^{a,*}, Ting Shi^a, Xin Li^b, Kangle Lv^a, Mei Li^a, Fangling Liu^a, Hongying Li^a, Ming Lei^a

^a Key Laboratory of Catalysis and Materials Science of the State Ethnic Affairs Commission & Ministry of Education, South-Central University for Nationalities, Wuhan 430074, PR China

^b College of Materials and Energy South China Agricultural University, Guangzhou 510642, PR China



ARTICLE INFO

Keywords:
CdS
Cd(OH)₂
Photocatalysis
Hydrogen production

ABSTRACT

In the past decade, photocatalytic H₂ production over CdS semiconductor has garnered considerable interest due to its visible-light response, suitable band structure, and controllable morphologies. To pursue higher photocatalytic efficiency and more feasibility for practical industrial applications, Cd(OH)₂ nanoparticle decorated CdS rod composites were designed and successfully fabricated in this study by a facile one-step hydrothermal method in strong alkali NaOH solution. The synthesis process followed a “mother liquor circulation” criteria since no NaOH was lost during the whole preparation course, which could greatly save costs and be conducive to the realization of large-scale production. When the content of Cd(OH)₂ was 17.6 mol% in the obtained composite, the photocatalytic H₂ production rate reached the highest (579.0 μmol h⁻¹) with the help of 0.6 wt% platinum (Pt), which was more than 386 and 15 times higher than that of Pt/Cd(OH)₂ and Pt/CdS, respectively. It was evidenced that such surprising and prominent enhancement of photoactivity was mainly attributed to the presence of Cd⁰ as an electron transport intermediary, which was produced by in-situ photoreduction of Cd(OH)₂ interfacial layer between CdS and Pt. This work could not only highlight the significant roles of Cd(OH)₂ on invigorating the photoactivity of CdS for H₂ production, but also open an avenue of using the concept of mother liquor circulation in the photocatalyst synthesis process to satisfy the industrial manufacture requirement.

1. Introduction

In modern times, excessive use of fossil fuels by human beings has caused both energy shortages and resource waste, accompanied by serious environmental pollution. One of effective ways to solve these problems is replacing fossil fuels with green, pollution-free hydrogen (H₂) energy [1,2]. However, the H₂-production technologies used in current industries still directly or indirectly rely on non-renewable resources, which are neither environmentally friendly nor economical. In 1972, as a milestone, the discovery of photocatalytic water splitting technology over TiO₂ electrode offered a new way to produce valuable H₂ energy via renewable solar energy over semiconductor materials [3]. Since then, efficient photocatalyst systems have been extensively explored [4–8].

The advancement of a high-efficiency photocatalyst requires two important aspects: light harvesting ability and charge separation efficiency [9,10]. In the solar radiation that can be received by the earth, visible light accounts for about 43% of the total energy, while ultraviolet (UV) light only accounts for 4%. Therefore, visible-light-driven semiconductor photocatalysts attracts much more interest than

traditional UV-light-driven ones in recent years [11–14]. Especially, cadmium sulfide (CdS) with a narrow bandgap of 2.4 eV and a negative enough conductive band (CB) edge potential is an attractive native candidate for visible-light-driven photocatalytic H₂ production [15–17]. However, every one has its weak side. The quick recombination of photogenerated charge carriers in the bulk and on the surface of CdS material usually exists and largely prohibits its wide applications. To solve this intrinsic problem, many approaches have been proposed to enhance the charge separation efficiency and photocatalytic activity of CdS, including controlling the morphology [18–23], deposition of noble or non-noble metal cocatalysts [24–32], construction of heterogeneous semiconductors [33–36], and so on.

On the one hand, the photocatalytic H₂ production efficiency of CdS could be directly affected by its geometrical morphology and surface structure. Particularly, one-dimensional (1D) materials including nanorods [37], nanowires [18], nanotubes [38] and nanobelts [39,40] provide a shorter bulk-to-surface diffusion distance than irregular particles for the photogenerated charge carriers, and thus suppress the electron-hole recombination in the bulk. On the other hand, deposition of cocatalysts could enhance the separation efficiency of

* Corresponding author.

E-mail addresses: liqin0518@mail.scuec.edu.cn, liqin0518@163.com (Q. Li).

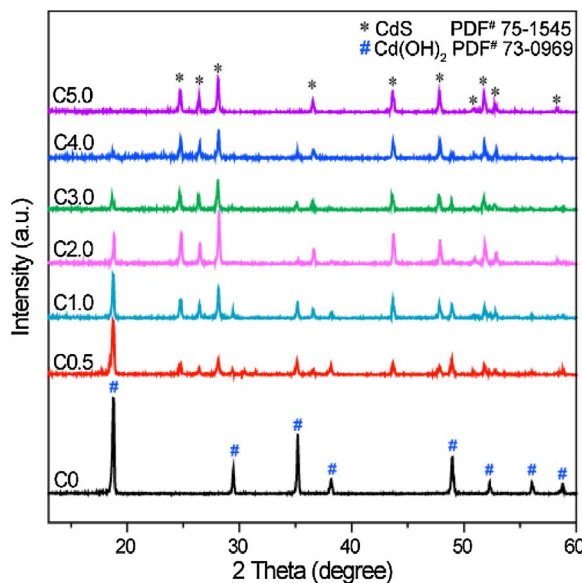


Fig. 1. XRD patterns of the C_x ($x = 0, 0.5, 1.0, 2.0, 3.0, 4.0$, and 5.0) samples.

photogenerated electrons and holes on the surface. Considering the high price and scarce resource of noble metals, non-noble metal based materials such as Cd [41,42], Ni [43], NiO [44], $\text{Ni}(\text{OH})_2$ [45], $\text{Cu}(\text{OH})_2$ [46] were more frequently utilized as cocatalysts in recent years [47]. For example, Wang et al. prepared Cd/CdS photocatalyst through a photochemical method using CdSO_4 and $\text{Na}_2\text{S}_2\text{O}_3 \cdot 5\text{H}_2\text{O}$ as precursors [41]. Superior photoactivity for H_2 production of Cd/CdS composite was observed than that of pure CdS. Shang et al. prepared Cd nanosheet by a low-temperature, low-cost polyol reduction method and then deposited CdS nanoparticles onto it through a oxidation-sulfurization process [42]. The Cd nanosheet reduced the aggregation of CdS nanoparticles, enhanced light absorbance, accelerated charge transfer, and consequently promoted the photocatalytic H_2 production efficiency of CdS. In addition, Yu's group successively prepared $\text{Ni}(\text{OH})_2\text{-TiO}_2$ [48], $\text{Cu}(\text{OH})_2\text{-TiO}_2$ [46] and $\text{Ni}(\text{OH})_2\text{-CdS}$ [45] composite photocatalysts, and verified the apparent promotion effect of these cocatalysts for photocatalytic H_2 production. Because the potentials of Ni^{2+}/Ni (-0.23 V) and Cu^{2+}/Cu (-0.224 V) in relation to the normal hydrogen electrode (NHE) are less negative than the CB levels of TiO_2 (-0.26 V vs. NHE) and CdS (-0.7 V vs. NHE), these transition metal hydroxides could accept electrons from the CB of semiconductor and be reduced to be metal atoms or clusters, which acted as a electron trapping center to promote the separation and transfer efficiency of charge carriers. From the thermodynamic point of view, the potential of Cd^{2+}/Cd (-0.403 vs. NHE) makes Cd-Cd(OH)₂ possess similar properties as Ni-Ni(OH)₂ and Cu-Cu(OH)₂ couples [49]. However, few researches reported on the

effect of Cd(OH)₂ cocatalyst on the photocatalytic H_2 -production performance of CdS [50].

Based on the previous works, we designed and successfully prepared Cd(OH)₂ nanoparticles decorated CdS rods photocatalyst through a facile one-step hydrothermal method in a strong alkali solution. Typically, 2 mmol of CdO was dissolved in a mixed aqueous solution of NaOH (16 M, 13 mL) and Na₂S (1 M, 2 mL). The mixture was stirred for 2 h at room temperature and then transferred into a Teflon-lined autoclave and held at 200 °C for 12 h. After that, the Teflon-lined autoclave was rapidly cooled to room temperature. The precipitates from the mixture were collected by centrifugation and then rinsed with water and ethanol for several times. The final product was dried in an oven at 80 °C overnight. In order to control the Cd(OH)₂ content and investigate its effect on the photocatalytic H_2 -production activity of the prepared Cd(OH)₂-CdS composite photocatalyst, the concentration of Na₂S aqueous solution was varied from 0 to 5.0 M. The resulting samples were labeled as C_x , where $x = 0, 0.5, 1.0, 2.0, 3.0, 4.0$, and 5.0 , respectively. It is pleasantly surprised to find that, with the help of a small quantity of Pt (0.6 wt%) as cocatalyst, a suitable amount of Cd(OH)₂ nanoparticles could tremendously enhance the photocatalytic H_2 production performance of Pt/CdS rods by 15 times. Series of characterizations were carried out to investigate the effects of Cd(OH)₂ on the physicochemical properties of CdS, and the enhancement mechanism was also deeply explored and proposed. It is anticipated that our work could inspire ongoing interest in exploring novel transition metal based cocatalysts to further enhance the photocatalytic performance of sulfide semiconductors and lower the cost of photocatalysis technology.

2. Results and discussion

2.1. Phase structure and chemical composition

Powder X-ray diffraction (XRD) patterns were recorded for the C_x ($x = 0, 0.5, 1.0, 2.0, 3.0, 4.0$, and 5.0) powders to confirm their crystallographic phase. The results are shown in Fig. 1. Typically, for the C_0 sample, all diffraction peaks can be readily indexed to pure Cd(OH)₂ (PDF 73-0969). With increasing x value, the co-existence of two crystalline phases (i.e. CdS (PDF 77-2306) and Cd(OH)₂ (PDF 73-0969)) can be observed for the C_x ($x = 0.5, 1.0, 2.0, 3.0$, and 4.0) samples. When $x = 5.0$, all diffraction peaks are indexed to CdS, indicating the phase purity of CdS. The XRD result demonstrated that Cd(OH)₂-CdS composite materials could be obtained using CdO and Na₂S as precursors under strong alkali condition. Furthermore, Material Analysis Using Diffraction (MAUD) was employed to calculate the phase composition of these samples [51], and the result was presented in Table 1. With increasing x value from 0 to 5.0, the CdS content gradually increased from 0 to 100% at the expense of the decreasing Cd(OH)₂ content. When $x = 1.0$, the calculated Cd(OH)₂ content in the composite was 12.3 mol%.

Table 1
Effects of Na₂S concentration on photoactivity and physicochemical properties of the C_x ($x = 0, 0.5, 1.0, 2.0, 3.0, 4.0$, and 5.0) samples.

Samples	Calculated Cd(OH) ₂ content (mol%) ^a	Detected Cd(OH) ₂ content (mol%) ^b	S_{BET} ($\text{m}^2 \text{g}^{-1}$) ^c	H_2 production rate ($\mu\text{mol h}^{-1}$)	QE(%) ^d
C_0	100	100	13.0	1.5	0
$C_{0.5}$	80.4	68.1	23.9	85.0	2.5
$C_{1.0}$	12.3	17.6	19.8	579.0	16.3
$C_{2.0}$	9.8	11.3	15.4	510.0	14.2
$C_{3.0}$	6.6	8.1	12.0	162.5	4.5
$C_{4.0}$	4.0	4.0	8.6	68.5	2.0
$C_{5.0}$	0	0	4.9	37.5	1.0

^a The calculated Cd(OH)₂ contents in the samples were obtained using a method of MAUD.

^b The detected Cd(OH)₂ contents in the samples were converted from the measured mass fractions of O atoms in the composites by CHNS/O elemental analyzer.

^c S_{BET} refers to the Brunauer-Emmett-Teller (BET) specific surface area.

^d QE refers to the apparent quantum efficiency.

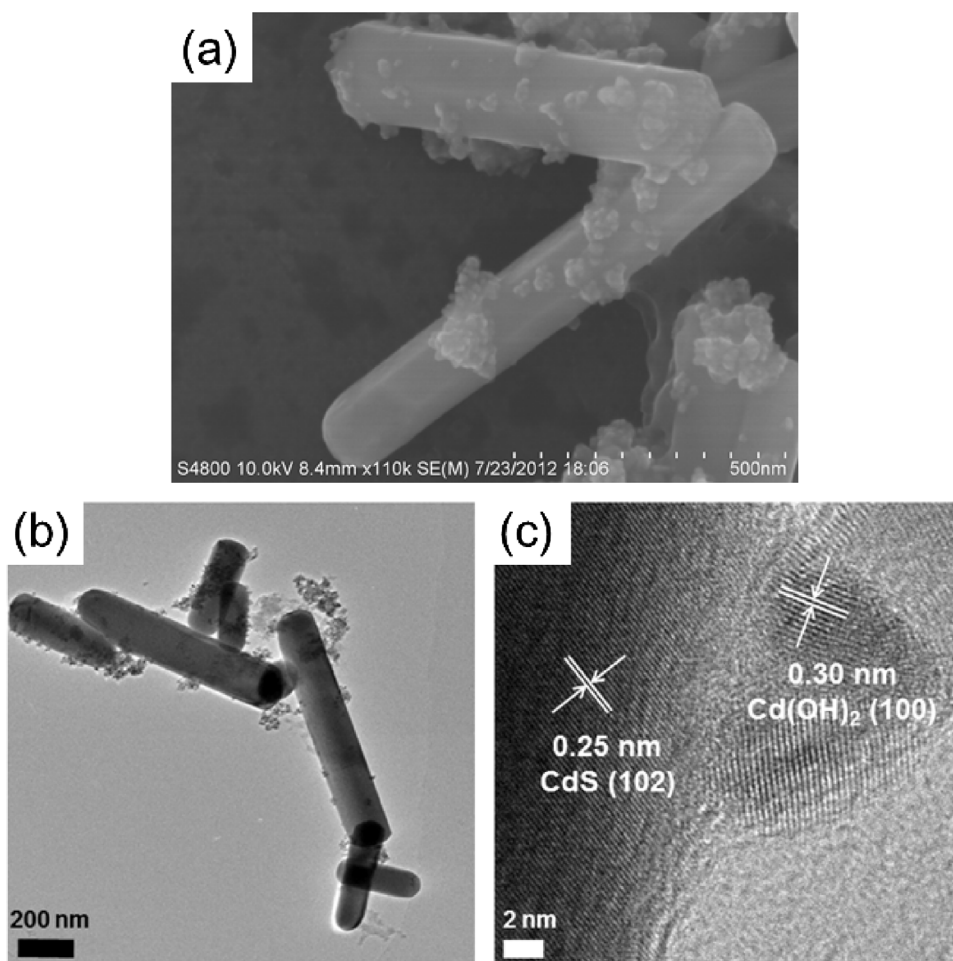


Fig. 2. (a) SEM, (b) TEM, and (c) HRTEM images of the C1.0 sample.

In order to further confirm the chemical composition of the samples, CHNS/O elemental analysis was carried out to detect the mass fractions of S and O atoms in the $\text{Cd}(\text{OH})_2\text{-CdS}$ composites. It was shown that the S mass fractions of the C_x ($x = 0, 0.5, 1.0, 2.0, 3.0, 4.0$, and 5.0) samples were $0, 7.0, 18.2, 19.7, 20.4, 21.4, 22.2\%$, respectively, while the O mass fractions were $21.9, 15.0, 3.9, 2.5, 1.8, 0.9$, and 0.02% , respectively. The O mass fraction results were converted into the molar contents of $\text{Cd}(\text{OH})_2$ and were listed in Table 1. When $x = 1.0$, the $\text{Cd}(\text{OH})_2$ content in the composite was 17.6 mol\% , which should be more accurate than the calculated value by MAUD.

2.2. Morphology and speculated forming process

The morphology observation over the prepared samples has been achieved through electron microscopy. Fig. S1 displays the scanning electron microscopy (SEM) images of the C_x ($x = 0, 0.5, 1.0, 3.0$, and 5.0) samples. The C0 sample (pure $\text{Cd}(\text{OH})_2$) appeared as a stack of hexagon nanosheets [52]. When $x = 0.5\text{--}3.0$, the samples consisted of rods and nanoparticles, and with increasing x value, the relative content of nanoparticles in the composites decreased. Combined with the change discipline of XRD peak intensities shown in Fig. 1, we intuitively guessed that the ingredient of the nanoparticles were $\text{Cd}(\text{OH})_2$. When $x = 5.0$, the samples consisted of large-sized particles and rods, which belonged to CdS according to the XRD result.

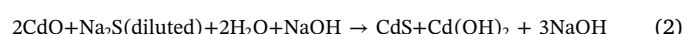
Furthermore, the morphology of the C1.0 sample was specifically concerned. SEM (Fig. 2a) and transmission electron microscopy (TEM) images (Fig. 2b) of the C1.0 sample show that it has a rod-like morphology with a diameter of ca. 200 nm. The surface of the rod is rough due to the adhering nanoparticles. To verify the component of the

rod and nanoparticle, the high-resolution transmission electron microscopy (HRTEM) image (Fig. 2c) and the energy dispersive X-ray spectroscopy (EDS) mapping (Fig. 3) of the C1.0 sample were carefully analyzed. In Fig. 2c, the lattice fringes with d spacing of ca. 0.25 and 0.30 nm can be assigned to the (102) and (100) lattice planes of the CdS and $\text{Cd}(\text{OH})_2$, respectively, indicating that the rod and nanoparticles could be referred to CdS and $\text{Cd}(\text{OH})_2$, respectively. Further evidence comes from the EDS mapping in Fig. 3, which displays that the Cd and S atoms were distributed on the whole rod, while the O atoms were mainly positioned at the nanoparticles on the surface of the rod. The corresponding EDS spectrum over the whole area in Fig. 3a was provided in the supporting information (Fig. S2).

According to the component analysis and morphology observation of the samples, the tentative chemical reactions occurred in the hydrothermal process is speculated. When there was no sulfur source (Na_2S) in the hydrothermal system, the reaction proceeded as follows:



In this case, the Cd^{2+} ions were dissolved from CdO and then precipitated as a hydroxide in the alkaline solution. Without Na_2S , the product was only $\text{Cd}(\text{OH})_2$. When the concentration of Na_2S in the hydrothermal system was low ($x = 0.5\text{--}4.0$), the reaction proceeded as follows:



In this case, the products consisted of CdS and $\text{Cd}(\text{OH})_2$. With increasing concentration of Na_2S , the yield of $\text{Cd}(\text{OH})_2$ decreased. When the concentration of Na_2S was high enough ($x = 5.0$), the reaction proceeded as follows:

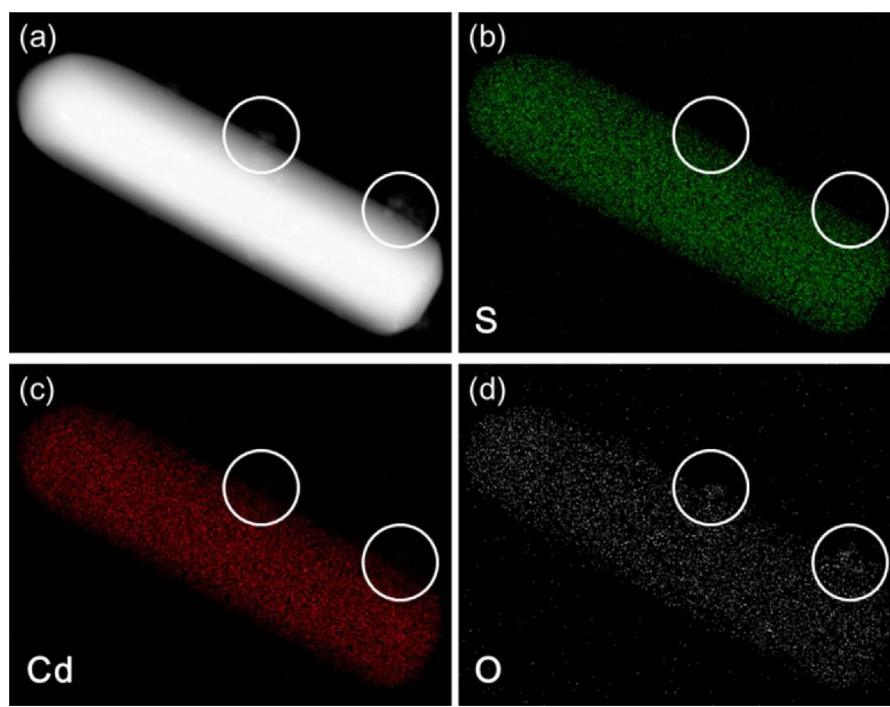


Fig. 3. (a) The S/TEM image of the C1.0 sample and the EDS mapping of its (b) S, (c) Cd, and (d) O atoms.

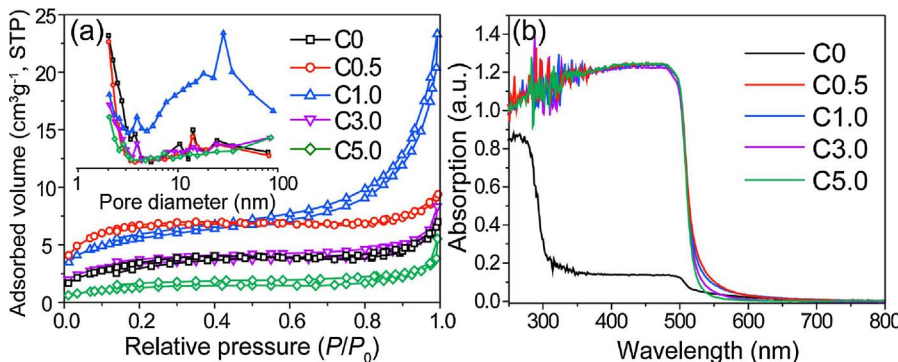
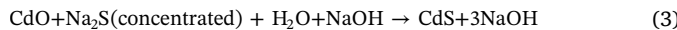


Fig. 4. (a) Nitrogen adsorption-desorption isotherms and corresponding pore size distribution curves (inset) and (b) UV-vis diffuse reflectance spectra of the Cx ($x = 0, 0.5, 1.0, 3.0$, and 5.0) samples. (For interpretation of the references to colour in text, the reader is referred to the web version of this article).



In this case, the product was only CdS. It is worthy to note that there is no loss of NaOH during the whole reaction process, indicating that such synthesis method follows the “mother liquor circulation” criteria, which could greatly save costs and be conducive to the realization of large-scale production.

2.3. Specific surface area and UV-vis diffused reflectance spectra

The Brunauer-Emmett-Teller (BET) specific surface area (S_{BET}) and pore structure of the prepared samples were investigated using adsorption-desorption measurements, and the results were summarized in Table 1. Typically, for the C0 sample with a hexagon-nanosheet shape (see Fig. S1a), the S_{BET} is $13.0 \text{ m}^2 \text{ g}^{-1}$. For other Cx samples with rod-like morphology (see Fig. S1b–e), it gradually decreases from 23.9 to $4.9 \text{ m}^2 \text{ g}^{-1}$ with x value increasing from 0.5 to 5. It is because nanoparticles always afford much larger S_{BET} than bulk materials, but the amount of the Cd(OH)_2 nanoparticles on the surface of CdS rod gradually decreased with increasing CdS content in the prepared Cd(OH)_2 -CdS composite. The nitrogen adsorption-desorption isotherms (Fig. 4a) showed that all the samples have an isotherm of type IV according to

the Brunauer-Deming-Deming-Teller (BDDT) classification, indicating the presence of mesopores (2–50 nm) [53]. The corresponding curves of the pore size distribution (inset of Fig. 4a) displayed that the C1.0 sample has a large amount of mesopores with a peak pore diameter of around 30 nm, which was formed by the relatively tight and large amount of contact between Cd(OH)_2 nanoparticles and CdS rods in the C1.0 sample. For other samples, differently, the diameter of most pores was less than 3 nm, which was mainly formed by the accumulation of primary nanoparticles in the Cd(OH)_2 particles and CdS rods.

To investigate the effect of Cd(OH)_2 content on the band structure of CdS, the UV-vis diffuse reflectance spectra (DRS) of the Cx ($x = 0.5, 1.0, 3.0$, and 5.0) samples are conducted and displayed in Fig. 4b. It can be seen that the absorption edges of all the samples except C0 remained nearly the same, indicating that the existence of Cd(OH)_2 nanoparticles have no impact on the band structure of CdS. However, the intensity of shoulder peak becomes higher with the increasing Cd(OH)_2 content. Such shoulder peak might be resulted from sub-bands or surface states caused by the presence of Cd(OH)_2 on the CdS surface [42]. In addition, the DRS spectrum of the C5.0 sample told that the obtained CdS had a direct bandgap energy (E_g) of 2.42 eV according to the Kubelka-Munk (KM) method (see Supporting information, Fig. S3) [54,55]. Therefore, the CB edge position of CdS in relation to NHE was calculated to be

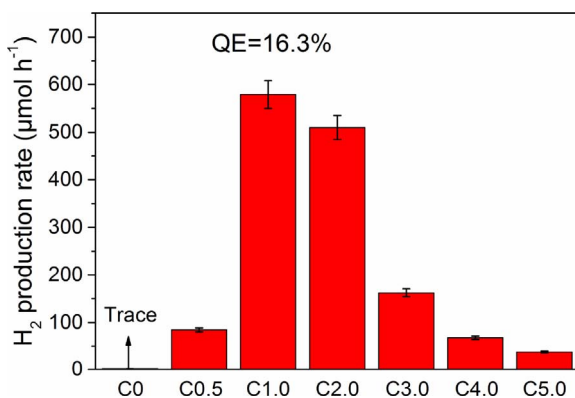


Fig. 5. Comparison of the visible-light photocatalytic activity of the Cx ($x = 0, 0.5, 1.0, 2.0, 3.0, 4.0$, and 5.0) samples for the H_2 production using mixed Na_2S (0.35 M) and Na_2SO_3 (0.25 M) aqueous solution as sacrificial reagent and 0.6 wt% Pt as cocatalyst; a 350 W Xenon arc lamp with a cutoff filter (≥ 420 nm) was used as the light source.

– 0.413 V according to the following equation:

$$E_{\text{CB}} = \chi - E^{\text{C}} - \frac{1}{2}E_{\text{g}} \quad (4)$$

where E_{CB} and χ are the CB edge potential and electronegativity of the CdS semiconductor, respectively, and $E^{\text{C}} = 4.5$ V, which is the energy of free electrons on the hydrogen scale. The detailed calculation method can be referred to our previous work [46,56].

2.4. Photocatalytic performance

Fig. 5 shows the comparison of the photocatalytic activity of the Cx ($x = 0, 0.5, 1.0, 2.0, 3.0, 4.0$, and 5.0) samples for the H_2 production under visible-light irradiation (≥ 420 nm) with 0.6 wt% Pt as cocatalyst, and the H_2 production rates and the apparent quantum efficiency (QE) of the samples were summarized in Table 1. It can be clearly seen that the Na_2S concentration has a significant impact on the photoactivity of the samples. When no Na_2S was added in the system, the H_2 production efficiency of the obtained C0 sample was negligible ($1.5 \mu\text{mol h}^{-1}$), indicating that Cd(OH)_2 itself had nearly no photoactivity for H_2 production. With the increment of Na_2S concentration, the H_2 production rate rapidly enhanced and reached the highest value of $579.0 \mu\text{mol h}^{-1}$ when $x = 1.0$ (for the C1.0 sample), with the

corresponding QE of 16.3% at 420 nm. However, further increase of Na_2S concentration decreased the H_2 production rate. When $x = 5.0$, the H_2 production rate was only $37.5 \mu\text{mol h}^{-1}$. Combined with the XRD result of the samples (Fig. 1 and Table 1), it suggests that the ratio of Cd(OH)_2 to CdS in the composites is significant for the improvement of the photocatalytic activity of CdS. Particularly, when the Cd(OH)_2 content was 17.6% for the C1.0 sample, the photocatalytic activity of H_2 production reached the maximum, which was more than 386 and 15 times higher than that of Cd(OH)_2 (i.e. the C0 sample) and CdS (i.e. the C5.0 sample), respectively.

2.5. Enhancement mechanism

In order to understand the specific reason of the promotion effect of Cd(OH)_2 nanoparticles on the CdS rods, three contrast experiments on the C1.0 and C5.0 samples were carried out. First, to investigate the component change of the sample after the photocatalytic H_2 production reaction, XRD patterns were reported on the recycled C1.0 sample after 1 h and 15 h-irradiation. As shown in Fig. 6a and Table 2, the Cd(OH)_2 content in the C1.0 sample obviously decreased from 17.6% to 7.5% after 1 h-irradiation, and totally disappeared after 15 h-irradiation. On the contrary, the XRD peak corresponding to Cd0 (PDF 05-0674) appeared and enhanced with the light irradiation proceeding. It can be deduced that part of Cd^{2+} ions were dissociated from Cd(OH)_2 in the complex and then in-situ photoreduced by the CdS-generated electrons to form Cd clusters. The existence of Cd metal nanoparticles on the CdS rods might be beneficial for the enhancement of charge carriers separation and transfer efficiency, which could be verified by the surface photovoltage (SPV) and transient photocurrent response over the C1.0 and C5.0 samples. As shown in Fig. 6b, the C1.0 and C5.0 samples displayed an obvious SPV response ranging from 300 to 600 nm. The SPV response edge of the C1.0 sample was similar to the band edge of CdS (the blue line comes from the DRS result of the C1.0 sample, Fig. 4b), implicating that the SPV signal of CdS semiconductor was mainly attributed to its band-band electronic transition [4]. With the introduction of Cd(OH)_2 , the SPV response of the C1.0 sample was strengthened apparently than that of bare CdS, indicating that the formed Cd metal clusters promoting the charge carriers separation and transfer on the surface of CdS rods. Similar phenomenon was also observed on the photocurrent response result (Fig. 6c).

Second, to further trace and inspect the effect of Cd metal on the

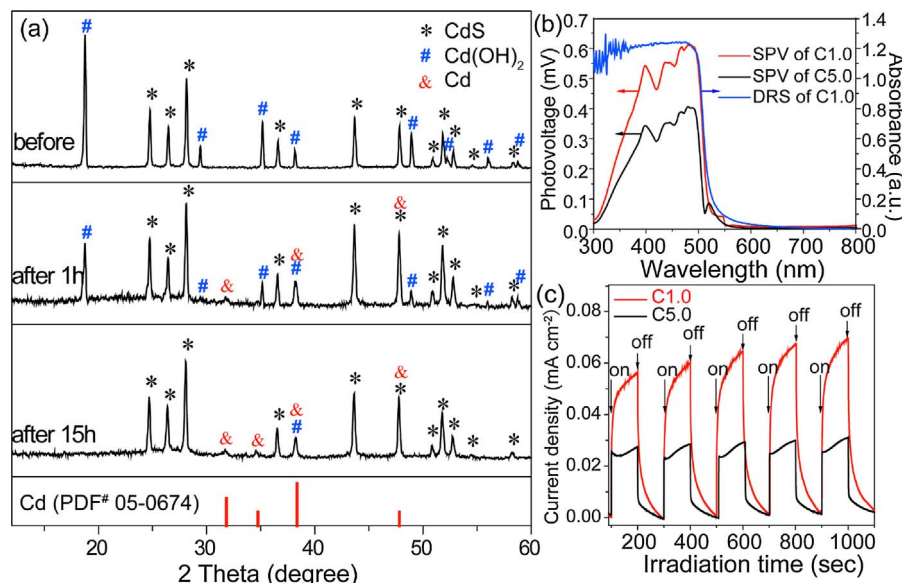


Fig. 6. (a) XRD patterns of the C1.0 sample before and after 1 h and 15 h irradiation. Comparison of (b) the SPV spectra and (c) the transient photocurrent responses of the C1.0 and C5.0 samples.

Table 2

The component of the C1 sample before and after the photocatalytic H₂ production for 1 h and 15 h.

Irradiation time	Cd(OH) ₂ (mol%) ^a
0 h	17.6
1 h	7.5
15 h	0

^a Cd(OH)₂ contents were converted from the measured mass fractions of O atoms in the composites by CHNS/O elemental analyzer.

photoactivity of CdS during long-time irradiation, the recycling photocatalytic H₂ production activities of the C1.0 and C5.0 samples in the presence of Pt cocatalyst were compared under visible-light irradiation for 6 h. It can be seen from Fig. 7a that the photocatalytic H₂ production rate of the C5.0 sample was maintained nearly the same during the 6 h-irradiation, whilst there was a rapid increase and then a slow decline in the change process over the C1.0 sample. Even so, the photocatalytic H₂ production efficiency of C1.0 sample after 6 h irradiation was still much higher than that of C5.0. According to the result in the first experiment (Fig. 6), such difference in the change discipline of photoactivity over the C1.0 and C5.0 samples during long-time irradiation could be reasonably explained. In the CdS-Cd(OH)₂ composite (the C1.0 sample), Cd was gradually produced under irradiation and increased the visible-light absorbance as well as electron conductivity of the composite, thus improving the photocatalytic activity. However, over-loaded Cd metals shielded part of CdS surface and decreased the amount of electrons involved in the H₂-production reaction. Therefore, the photoactivity show a certain degree of decline.

Third, to survey the synergistic effect of Pt and Cd(OH)₂ in the photocatalysis process, the photocatalytic H₂ production rates of the

C1.0 and C5.0 samples with and without Pt cocatalyst were compared. Based on the result as shown in Fig. 7b, the following three conclusion could be drawn: (1) Without the assistant of Pt cocatalyst, the photocatalytic activity of C1.0 was obviously lower than that of C5.0. It is because the produced Cd° from the reduction of Cd(OH)₂ has a high overpotential for H₂ production, which decreased the photoactivity of CdS [57]. (2) With the help of Pt, the photoactivities of both C1.0 and C5.0 samples were enhanced to a large level. It is because the H⁺ prefers to be reduced to form H₂ over Pt with a very low overpotential for H₂ production [27]. More significantly, Pt as a noble metal with a good electron conductivity could effectively separate the photo-generated electron-hole pairs on the surface of CdS, and consequently enhance the photocatalytic H₂ production efficiency [58]. (3) In the presence of Pt, the photoactivity of sample C1.0 was enhanced dramatically and even surpassed that of sample C5.0 to a large degree. The joint conclusions declared that the Cd(OH)₂ could remarkably enhance the photocatalytic H₂ production activity of CdS with the help of Pt.

According to the above investigations, the mechanism of photocatalytic H₂ production process over the prepared Cd(OH)₂-CdS composite was proposed. Firstly, electrons and holes were excited from CdS semiconductor under visible-light irradiation (Reaction (5)). Since the CB edge of CdS (-0.413 V vs. NHE) was more negative than the reduction potential of Cd²⁺/Cd° (-0.403 V vs. NHE), the electrons on the CdS surface could reduce Cd²⁺ ions into Cd° clusters (Reaction (7)), where the Cd²⁺ ions were dissociated from Cd(OH)₂ nanoparticles on the surface of CdS (Reaction (6)). The formed Cd clusters acted as interfacial transfer mediator to promote the separation efficiency of electron-hole pairs and delivered electrons onto the surface of Pt, where the surrounding H⁺ was finally reduced to be H₂ (Reaction (8)). Corresponding mechanism scheme of photocatalytic H₂ production process occurring on the Cd(OH)₂-CdS composite with Pt as cocatalyst was illustrated in Fig. 8.

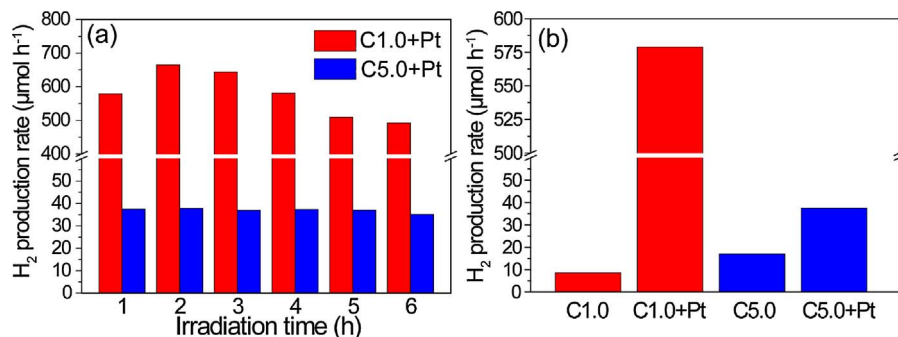


Fig. 7. (a) Time course of photocatalytic H₂ production over the C1.0 sample under visible-light irradiation with 0.6 wt% Pt as cocatalyst. (b) Comparison of photocatalytic H₂ production rates of sample C1.0 and C5.0 with and without Pt cocatalyst.

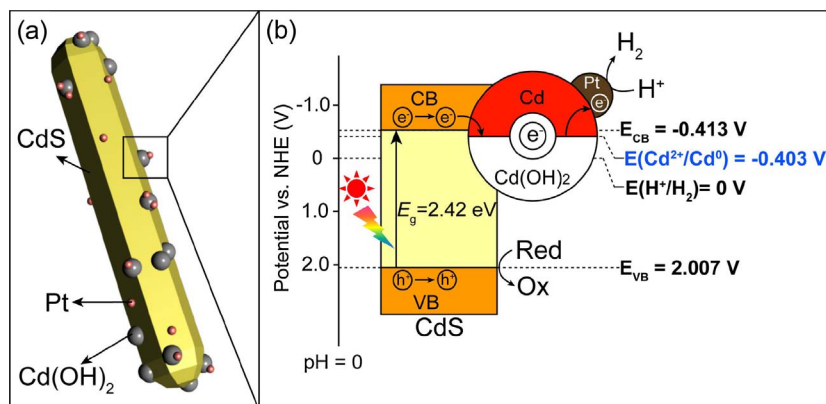
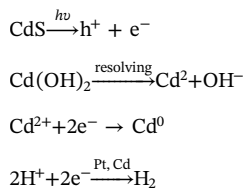


Fig. 8. (a) Three dimensional illustration of Pt/Cd(OH)₂ codecorated CdS rod and (b) mechanism of photocatalytic H₂ production process on the prepared Pt/Cd(OH)₂-CdS composite photocatalyst.



3. Conclusions

In summary, Cd(OH)_2 nanoparticle decorated CdS rod composites were successfully fabricated using CdO and Na_2S as the precursors through a facile one-step hydrothermal method in a strong alkaline NaOH aqueous solution. The influence of Cd(OH)_2 content on the physico-chemical properties and visible-light photocatalytic H_2 production activity of CdS was systematically investigated. The results showed that the photocatalytic H_2 production rate of the composite in the presence of 0.6 wt% Pt reached the highest ($579.0 \mu\text{mol h}^{-1}$) when the molar content of Cd(OH)_2 was 17.6%, which was more than 386 and 15 times higher than that of Pt/Cd(OH)_2 and Pt/CdS , respectively. Control experiment results demonstrated that such remarkable enhancement was mainly attributed to the significant role of Cd clusters as the interfacial electron transfer mediator between CdS and Pt, which was formed from the in-situ reduction of Cd(OH)_2 by photogenerated electrons of CdS . This study may not only enable a wide development of Cd(OH)_2 cocatalyst-enhanced semiconductor photocatalysis for H_2 production, but also raise new concern on the optimization of synthesis process to meet industrial needs.

Acknowledgments

This work was supported by National Natural Science Foundation of China (21503281, 21571192), Fundamental Research Funds for the Central Universities (CZP17071, CZT18018), and Natural Science Foundation of South-Central University for Nationalities (YZZ14001, XTZ15016). Xin Li would like to thank National Natural Science Foundation of China (51672089) and the State Key Laboratory of Advanced Technology for Material Synthesis and Processing (Wuhan University of Technology) (2015-KF-7) for their support.

Appendix A. Supplementary data

Supplementary material related to this article can be found, in the online version, at doi:<https://doi.org/10.1016/j.apcatb.2018.01.078>.

References

- [1] R.D. Cortright, R.R. Davda, J.A. Dumesic, *Nature* 418 (2002) 964–967.
- [2] J.W. Yu, B.C. Zhu, W. You, M. Jaroniec, J.G. Yu, *Appl. Catal. B: Environ.* 220 (2018) 148–160.
- [3] A. Fujishima, K. Honda, *Nature* 238 (1972) 37–38.
- [4] Y. Xia, Q. Li, K.L. Lv, D.G. Tang, M. Li, *Appl. Catal. B: Environ.* 206 (2017) 344–352.
- [5] X. Li, J.G. Yu, J.X. Low, Y.P. Fang, J. Xiao, X.B. Chen, *J. Mater. Chem. A* 3 (2015) 2485–2534.
- [6] Q. Li, H. Meng, J.G. Yu, W. Xiao, Y.Q. Zheng, J. Wang, *Chem. Eur. J.* 20 (2014) 1176–1185.
- [7] M.H. Luo, P. Lu, W.F. Yao, C.P. Huang, Q.J. Xu, Q. Wu, Y. Kuwahara, H. Yamashita, *ACS Appl. Mater. Interfaces* 8 (2016) 20667–20674.
- [8] T. Kamegawa, K. Irikawa, H. Yamashita, *Sci. Rep.* 7 (2017) 13628.
- [9] Y. Xia, Q. Li, K.L. Lv, M. Li, *Appl. Surf. Sci.* 398 (2017) 81–88.
- [10] J.G. Yu, Q. Li, S.W. Liu, M. Jaroniec, *Chem. Eur. J.* 19 (2013) 2433–2441.
- [11] T. Takayama, I. Tsuji, N. Aono, M. Harada, T. Okuda, A. Iwase, H. Kato, A. Kudo, *Chem. Lett.* 46 (2017) 616–619.
- [12] G. Kim, S.H. Lee, W. Choi, *Appl. Catal. B: Environ.* 162 (2015) 463–469.
- [13] Y. Xia, Q. Li, X.F. Wu, K.L. Lv, D.G. Tang, M. Li, *Appl. Surf. Sci.* 391 (2017) 565–571.
- [14] Y. Park, W. Kim, H. Park, T. Tachikawa, T. Majima, W. Choi, *Appl. Catal. B: Environ.* 91 (2009) 355–361.
- [15] Q. Li, X. Li, S. Wageh, A. Al-Ghamdi, J.G. Yu, *Adv. Energy Mater.* (2015) 1500010.
- [16] J.F. Zhang, S. Wageh, A. Al-Ghamdi, J.G. Yu, *Appl. Catal. B: Environ.* 192 (2016) 101–107.
- [17] J.G. Yu, Y.F. Yu, P. Zhou, W. Xiao, B. Cheng, *Appl. Catal. B: Environ.* 156–157 (2014) 184–191.
- [18] J. Jin, J.G. Yu, G. Liu, P.K. Wong, *J. Mater. Chem. A* 1 (2013) 10927–10934.
- [19] X.L. Wang, Z.C. Feng, D.Y. Fan, F.T. Fan, C. Li, *Cryst. Growth Des.* 10 (2010) 5312–5318.
- [20] C.X. Li, L.J. Han, R.J. Liu, H.H. Li, S.J. Zhang, G.J. Zhang, *J. Mater. Chem.* 22 (2012) 23815–23820.
- [21] M. Chen, Y. Xie, J. Lu, Y.J. Xiong, S.Y. Zhang, Y.T. Qian, X.M. Liu, *J. Mater. Chem.* 12 (2002) 748–753.
- [22] H.B. Chu, X.M. Li, G.D. Chen, W.W. Zhou, Y. Zhang, Z. Jin, J.J. Xu, Y. Li, *Cryst. Growth Des.* 5 (2005) 1801–1806.
- [23] S. Ma, J. Xie, J.Q. Wen, K.L. He, X. Li, W. Liu, X.C. Zhang, *Appl. Surf. Sci.* 391 (2017) 580–591.
- [24] P. Wang, Y. Sheng, F.Z. Wang, H.G. Yu, *Appl. Catal. B: Environ.* 220 (2018) 561–569.
- [25] Q.X. Peng, D. Xue, S.Z. Zhan, C.L. Ni, *Appl. Catal. B: Environ.* 219 (2017) 353–361.
- [26] T.M. Di, B.C. Zhu, J. Zhang, B. Cheng, J.G. Yu, *Appl. Surf. Sci.* 389 (2016) 775–782.
- [27] Q. Li, B.D. Guo, J.G. Yu, J.R. Ran, B.H. Zhang, H.J. Yan, J.R. Gong, *J. Am. Chem. Soc.* 133 (2011) 10878–10884.
- [28] X. Zong, H.J. Yan, G.P. Wu, G.J. Ma, F.Y. Wen, L. Wang, C. Li, *J. Am. Chem. Soc.* 130 (2008) 7176–7177.
- [29] D. Lang, F.Y. Cheng, Q.J. Xiang, *Catal. Sci. Tech.* 6 (2016) 6207–6216.
- [30] J.S. Jang, D.J. Ham, N. Lakshminarasimhan, J.S. Lee, *Appl. Catal. A* 346 (2008) 149–154.
- [31] J. Choi, D. Amaranatha Reddy, N.S. Han, S. Jeong, S. Hong, D. Praveen Kumar, J.K. Song, T.K. Kim, *Catal. Sci. Tech.* 7 (2017) 641–649.
- [32] S. Hong, D.P. Kumar, D.A. Reddy, J. Choi, T.K. Kim, *Appl. Surf. Sci.* 396 (2017) 421–429.
- [33] J.Z. Su, T. Zhang, L. Wang, J.W. Shi, Y.B. Chen, *Chin. J. Catal.* 38 (2017) 489–497.
- [34] Y.J. Cui, *Chin. J. Catal.* 36 (2015) 372–379.
- [35] J. Jin, J.G. Yu, D.P. Guo, C. Cui, W.K. Ho, *Small* 11 (2015) 5262–5271.
- [36] A.Y. Meng, B.C. Zhu, B. Zhong, L.Y. Zhang, B. Cheng, *Appl. Surf. Sci.* 422 (2017) 518–527.
- [37] J.G. Yu, Y.F. Yu, B. Cheng, *RSC Adv.* 2 (2012) 11829–11835.
- [38] Y.J. Xiong, Y. Xie, J. Yang, R. Zhang, C.Z. Wu, G.A. Du, *J. Mater. Chem.* 12 (2002) 3712–3716.
- [39] J. Zhang, F.H. Jiang, L.D. Zhang, *J. Phys. Chem. B* 108 (2004) 7002–7005.
- [40] L. Li, P.C. Wu, X.S. Fang, T.Y. Zhai, L. Dai, M.Y. Liao, Y. Koide, H.Q. Wang, Y. Bando, D. Golberg, *Adv. Mater.* 22 (2010) 3161–3165.
- [41] Q.Z. Wang, J.J. Li, Y. Bai, J.H. Lian, H.H. Huang, Z.M. Li, Z.Q. Lei, W.F. Shang Guan, *Green Chem.* 16 (2014) 2728–2735.
- [42] L. Shang, B. Tong, H.J. Yu, G.I.N. Waterhouse, C. Zhou, Y.F. Zhao, M. Tahir, L.Z. Wu, C.H. Tung, T.R. Zhang, *Adv. Energy Mater.* 6 (2016) 1501241.
- [43] J.R. Ran, J. Zhang, J.G. Yu, S.Z. Qiao, *ChemSusChem* 7 (2014) 3426–3434.
- [44] X.P. Chen, W. Chen, P.B. Lin, Y. Yang, H.Y. Gao, J. Yuan, W.F. Shangguan, *Catal. Commun.* 36 (2013) 104–108.
- [45] J.R. Ran, J.G. Yu, M. Jaroniec, *Green Chem.* 13 (2011) 2708–2713.
- [46] J.G. Yu, J.R. Ran, *Energy Environ. Sci.* 4 (2011) 1364–1371.
- [47] J.R. Ran, J. Zhang, J.G. Yu, M. Jaroniec, S.Z. Qiao, *Chem. Soc. Rev.* 43 (2014) 7787–7812.
- [48] J.G. Yu, Y. Hai, B. Cheng, *J. Phys. Chem. C* 115 (2011) 4953–4958.
- [49] M.I. Litter, *Appl. Catal. B: Environ.* 23 (1999) 89–114.
- [50] A. Kumar, D.P.S. Negi, *J. Photochem. Photobiol. A* 134 (2000) 199–207.
- [51] L. Lutterotti, S. Matthies, H.R. Wenk, MAUD (material analysis using diffraction): a user friendly java program for rietveld texture analysis and more, Proceeding of the Twelfth International Conference on Textures of Materials (ICOTOM-12), Montreal, Canada, 1999, NRC Press: Ottawa, Canada, 1999, p. 1599.
- [52] H. Zhang, X.Y. Ma, Y.J. Ji, J. Xu, D.R. Yang, *Mater. Lett.* 59 (2005) 56–58.
- [53] K.S.W. Sing, D.H. Everett, R.A.W. Haul, L. Moscou, R.A. Peirotti, J. Rouquerol, *Pure Appl. Chem.* 54 (1982) 2201–2218.
- [54] E.M. Patterson, C.E. Shelden, B.H. Stockton, *Appl. Opt.* 16 (1977) 729–732.
- [55] N. Serpone, D. Lawless, R. Khairutdinov, *J. Phys. Chem.* 99 (1995) 16646–16654.
- [56] Q. Li, H. Meng, P. Zhou, Y.Q. Zheng, J. Wang, J.G. Yu, J.R. Gong, *ACS Catal.* 3 (2013) 882–889.
- [57] D.A. Corrigan, R.M. Bender, *J. Electrochem. Soc.* 136 (1989) 723–728.
- [58] Q. Li, C. Cui, H. Meng, J.G. Yu, *Chem. Asian J.* 9 (2014) 1766–1770.